Supplemental Material

Isotope sclerochronology indicates enhanced seasonal precipitation in northern South America (Colombia) during the Mid Miocene Climatic Optimum

This Supplemental Material Contains:

- Supplementary Discussion/Text
    - Locality information – Guajira Peninsula
    - Locality information – Other modern sites
    - Instrumental data – Global gridded datasets
    - Methods – Shell sampling
    - Methods – Isotopic sampling
- Supplementary Figures
    - Figure S1 – Maps of locations used for gridded dataset analysis
    - Figure S2 – Geologic map of Guajira Peninsula
    - Figure S3 – Composite stratigraphic column
    - Figure S4 – Shell sampling schematic
    - Figure S5 – Correlation between $\delta^{18}O$ and $\delta^{13}C$ in all shells
    - Figure S6 – $\delta^{18}O$ and $\delta^{13}C$ profiles of all shells
    - Figure S7 – Comparison between $\delta^{18}O$ range and environmental parameters
    - Figure S8 – Comparison between $\delta^{18}O$ range, shell size and lifespan
    - Figure S9 – Seasonal variation in sea surface temperatures, ERSST v. 5
    - Figure S10 – $\delta^{13}C$ profiles of all shells
    - Figure S11 - Correlation between range in $\delta^{13}C$ and range in $\delta^{18}O$
    - Figure S12 – Correlation between $\Delta\delta^{18}O_{sw}$ and precipitation
    - Figure S13 – Raman spectroscopy spectra
- Supplementary Tables
    - Table S1 – Sample IDs, STRI locality numbers, stratigraphic heights and calibrated ages for all measured specimens.
    - Table S2 – Raw $\delta^{18}O$ and $\delta^{13}C$ data for all shells [Separate Excel File]
    - Table S3 – Shell lifespan, size, and $\delta^{18}O$ and $\delta^{13}C$ range for all shells
    - Table S4 – Modern climate data for all sites
    - Table S5 – SEM imagery
- Additional References not cited in the main text

Supplementary Discussion – Sample Locality Information

GUAJIRA PENINSULA:
　　　Fossil samples were collected from various locations on the Guajira Peninsula from the Castilletes and Jimol Formations. These locations and sections are well described in other publications (Hendy et al., 2015; Moreno et al., 2015). Figures S1 and S2 in this supplement show a composite stratigraphic column displaying horizons from which fossil shells were collected, and a geologic map of the Peninsula with spatial distribution of sampling locations marked. Two modern samples were collected from coastal site 290628 (Figure S2). The modern isotopic difference between continental precipitation and seawater in this region is 4-6‰ (IAEA/WMO 2018).

OTHER MODERN LOCATIONS:
　　　Modern turritellids collected at other tropical sites nearby the fossil collection site on the Guajira Peninsula were chosen from the dry collections of the Museum of Zoology Research Museum Collections at University of Michigan. These shells were collected by varying donors over many years, and were often part of personal collections before being donated to the museum. Therefore, specific location data (e.g. a specific beach or town) was often not available. However, all shells had a country of origin at a minimum, and in some cases more information such as a nearby city. The representations on the map in Figure 1 represent our best guess as to the location of sample collection based on the limited data available, but some of these locations have significant uncertainties. This uncertainty in location is mitigated by comparing isotope profiles to satellite-derived sea surface and precipitation data, which average over a larger area and reflect regional conditions.

**Supplementary Discussion – Instrumental Data**

GRIDED DATASET SEA SURFACE TEMPERATURE (SST) AND PRECIPITATION DATA:
　　　Annual change and mean SST were calculated from NOAA ERSST v.5 dataset (Huang et al., 2017), over the regions shown in the maps to the right and below, highlighted by the red boxes. The same regions were used in calculation of precipitation data from the CRU 3.25 Global Precipitation dataset (Harris et al., 2014). In both cases, the region was averaged over using a latitude-weighted X-Y average, and the average monthly value was calculated for the period 1930-2012. Ranges in SST and precipitation were determined as the minimum to maximum monthly mean value. MAP was calculated by summing these means; seasonal variance was calculated by taking the difference of the highest and lowest (rainiest and driest, or warmest and coldest) months.
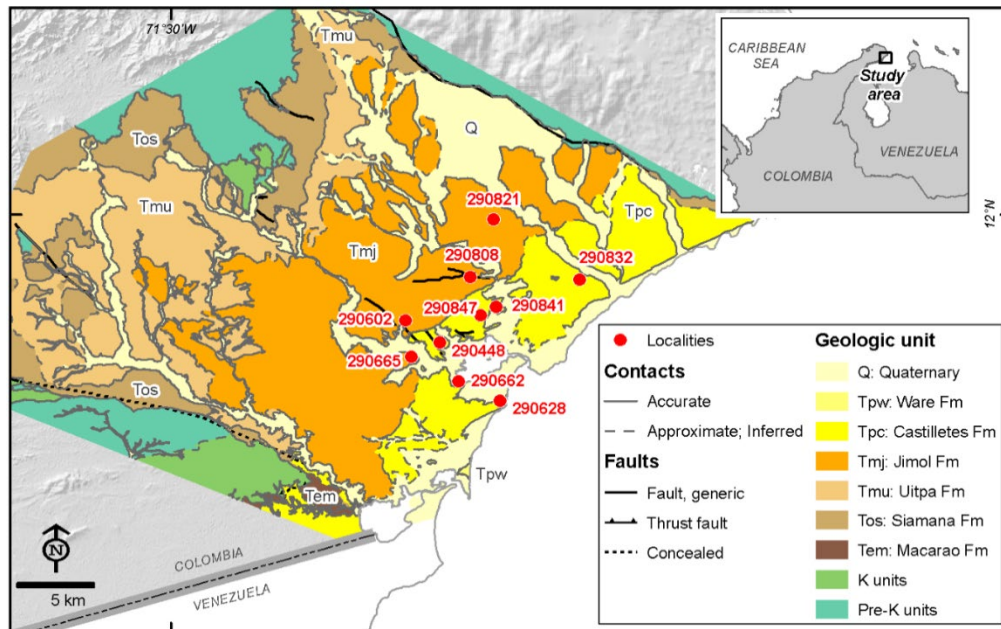
Supplemental Material Figure 1 (S1) –
Locations Used for Calculations with Gridded Datasets (right)
Red boxes show the latitude/longitude range defined for each modern site and carried forward into calculations of monthly average SSTs (NOAA ERSST v.5) and precipitation (CRU 3.25). The CRU 3.25 Global Precipitation dataset resolution is 0.5° x 0.5°, and the ERSST v.5 resolution is 2° × 2°.
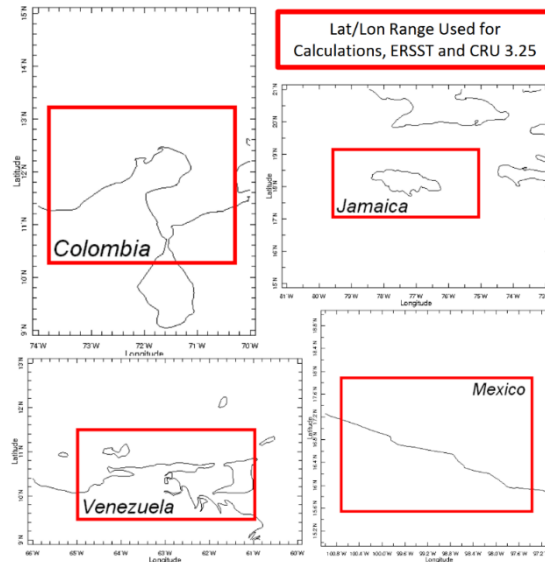

Supplemental Material Figure 2 (S2) – Geologic map of Guajira Peninsula with sampling locations
Geologic map of the sampling locations on the Guajira Peninsula, Colombia. Numbers are the STRI locality IDs, which correspond to the names of samples collected at that location. The modern samples were collected at coastal site 290628. Modified from Moreno et al., 2015.

Supplemental Material Figure 3 (S3) – Composite stratigraphic column with sample collection horizons

Composite stratigraphic column of the Jimol and Castilletes formation on the Guajira Peninsula, with labeled horizons showing the positions within the stratigraphy from which the 25 fossil *Turitella* samples were collected. Samples marked with *XRD are levels in the stratigraphy where samples underwent X-ray diffraction to assess preservation (not on the same samples as were analyzed for stable isotopes).
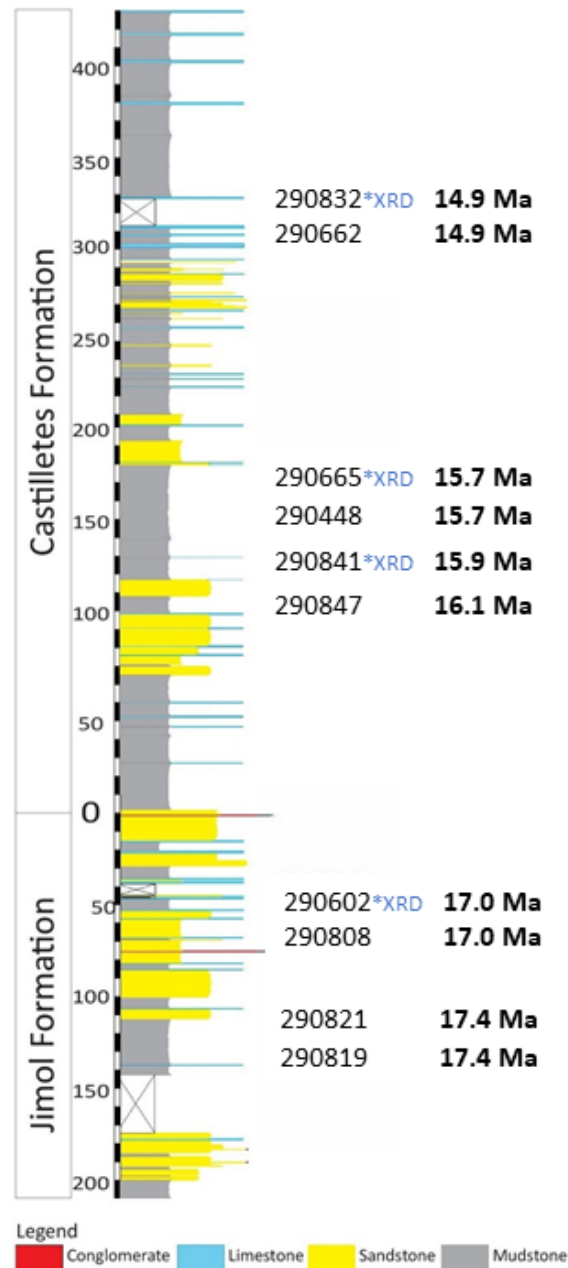
Supplementary Discussion - Methods

SHELL SAMPLING:
  Shells were sampled along the spiral growth direction, while recording cumulative distance from the apex for each sampling location. Each sample was taken from the middle of the whorl, equidistant to each side. The high-resolution sampling scheme is illustrated in the photo below (Figure S1). When the apex tip was broken, missing shell length was estimated using the Theoretical Apex System (TAS) method (Johnson et al., 2017), as employed by Anderson et al., (2017). 28 specimens underwent high-resolution drilling (3-12 samples/whorl, 40-50μg/sample), and 6 were sampled at coarser resolution (1 sample/whorl, ~10-40 μg/sample) using a handheld drill at low speed. All sampled carbonate powders were analyzed for their stable isotopic composition ($\delta^{18}O$ and $\delta^{13}C$). Based on resulting $\delta^{18}O$ cyclicity, shell lifespans were estimated to vary between <1 to 2 years as a minimum estimate (Table S2), in agreement with previous studies of Turritella (Allmon, 2011; Anderson et al., 2017).

Data Repository Figure 4 (S4) – Shell sampling schematic
Sampling method along the center of each whorl, as demonstrated with sample 290602-A. Sample is on 1cm graph paper for scale.
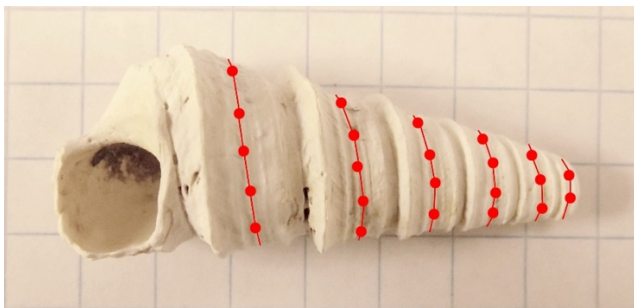
PRESERVATION ASSESSMENT:
  Raman spectroscopy was used on all fossil shells and one modern shell, and showed spectral peaks corresponding to pure aragonite (see figure S13). SEM imagery was taken of 13 fossil shells, spanning all ages and horizons, and showed the original aragonite shell fabric was intact, and similar in structure to modern samples (see Table S5). Shells from four horizons were analyzed for XRD and were found to contain 100% aragonite.
  Shells also preserve sinusoidal seasonal patterns in $\delta^{18}O$ that are unlikely to survive significant alteration. Partial recrystallization or contamination with secondary material would, if anything, mute the seasonal magnitude seen in $\delta^{18}O$ through regression to the mean: so, our conclusions about the increased magnitude in $\delta^{18}O$ seen in fossil shells compared to modern should be robust to minor alteration.

ISOTOPIC MEASUREMENTS:
  Stable isotopic analysis was conducted at both the University of Michigan and University of Florida. At University of Florida, samples were analyzed using a Kiel III carbonate preparation device attached to a Finnigan-MAT 252 mass spectrometer, with analytical error estimated to be ±0.03‰ for $\delta^{13}C$ and ±0.05‰ for $\delta^{18}O$ (n = 175) based on calibration to daily analysis of NBS-19. At University of Michigan, samples were analyzed using a Kiel IV device attached to a Thermo-MAT 253 mass spectrometer and were calibrated against NBS-19 and NBS-18 run daily. Analytical error on these measurements was better than ±0.1‰ for both $\delta^{13}C$ and $\delta^{18}O$. All $\delta^{13}C$ and $\delta^{18}O$ data are presented relative to Vienna Pee Dee Belemnite (VPDB).
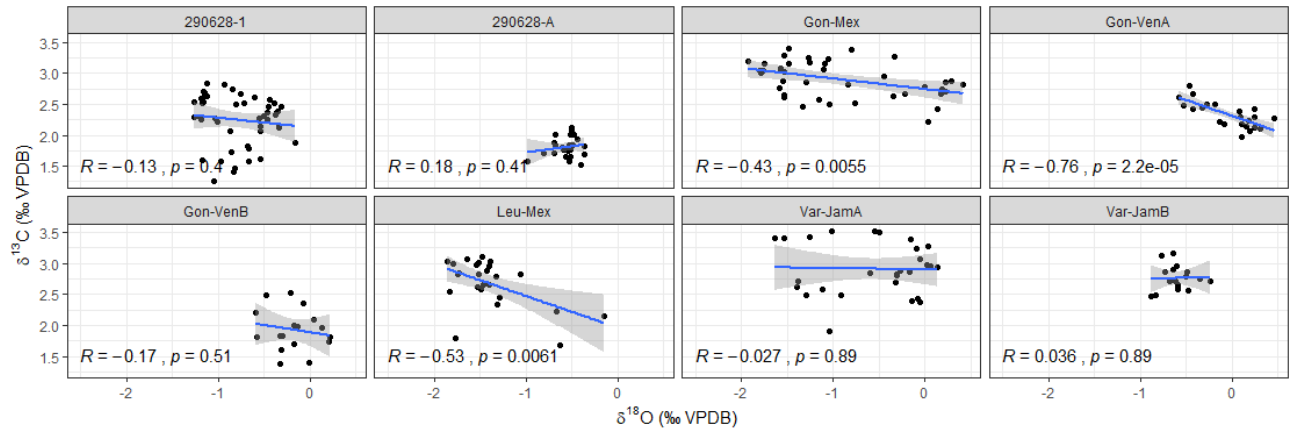
Supplemental Material Figure 5 (S5) – Correlation between $\delta^{18}O$ and $\delta^{13}C$ for all shells

Correlation of $\delta^{18}O$ and $\delta^{13}C$ values for all (A) fossil and (B) modern samples. Gray shaded area around each regression line represents the standard error of the fit. Out of 25 fossil shells analyzed, 9 showed significant positive correlation between $\delta^{18}O$ and $\delta^{13}C$, 4 showed significant negative correlation, and 12 had correlations that were not significant at the 0.05 p-value level. 18 out of the 25 shells (72%) show positive R values, which may indicate that they are influenced by freshening (Tao et al., 2013).

5A) Fossil shells
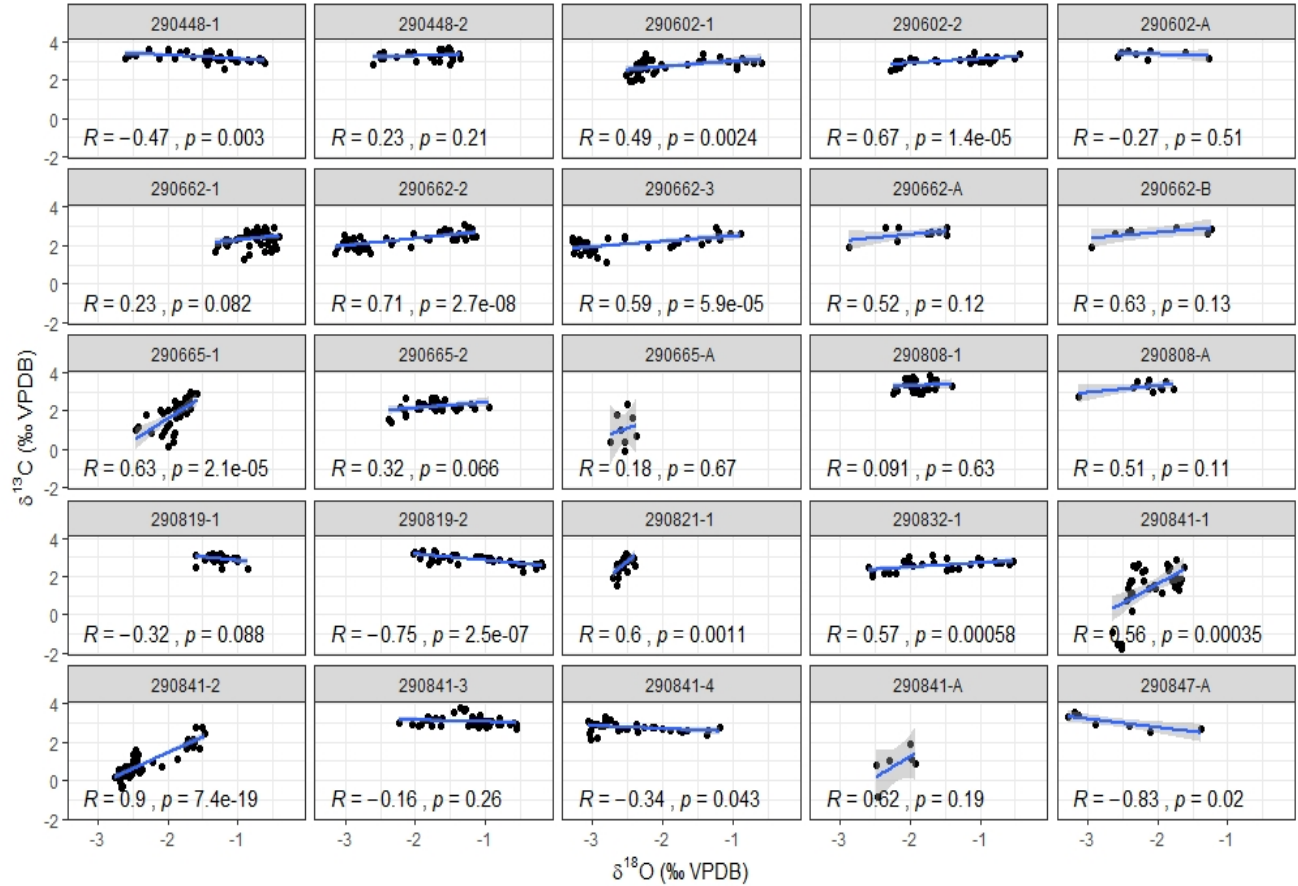
5B) Modern shells

Supplemental Material Figure 6 (S6) – δ^{18}O and δ^{13}C profiles for all shells

Individual δ^{18}O and δ^{13}C profiles for all (A) fossil and (B) modern samples, showing subannual variations. δ^{18}O data (black circles) plotted on the left y-axis, with values inverted. δ^{13}C data (blue line, triangles) plotted on the right y-axis (not inverted). X-axis shows the accumulated distance from the apex of the shell (0mm) to the aperture, along the spiral growth direction.

6A) Fossil specimens
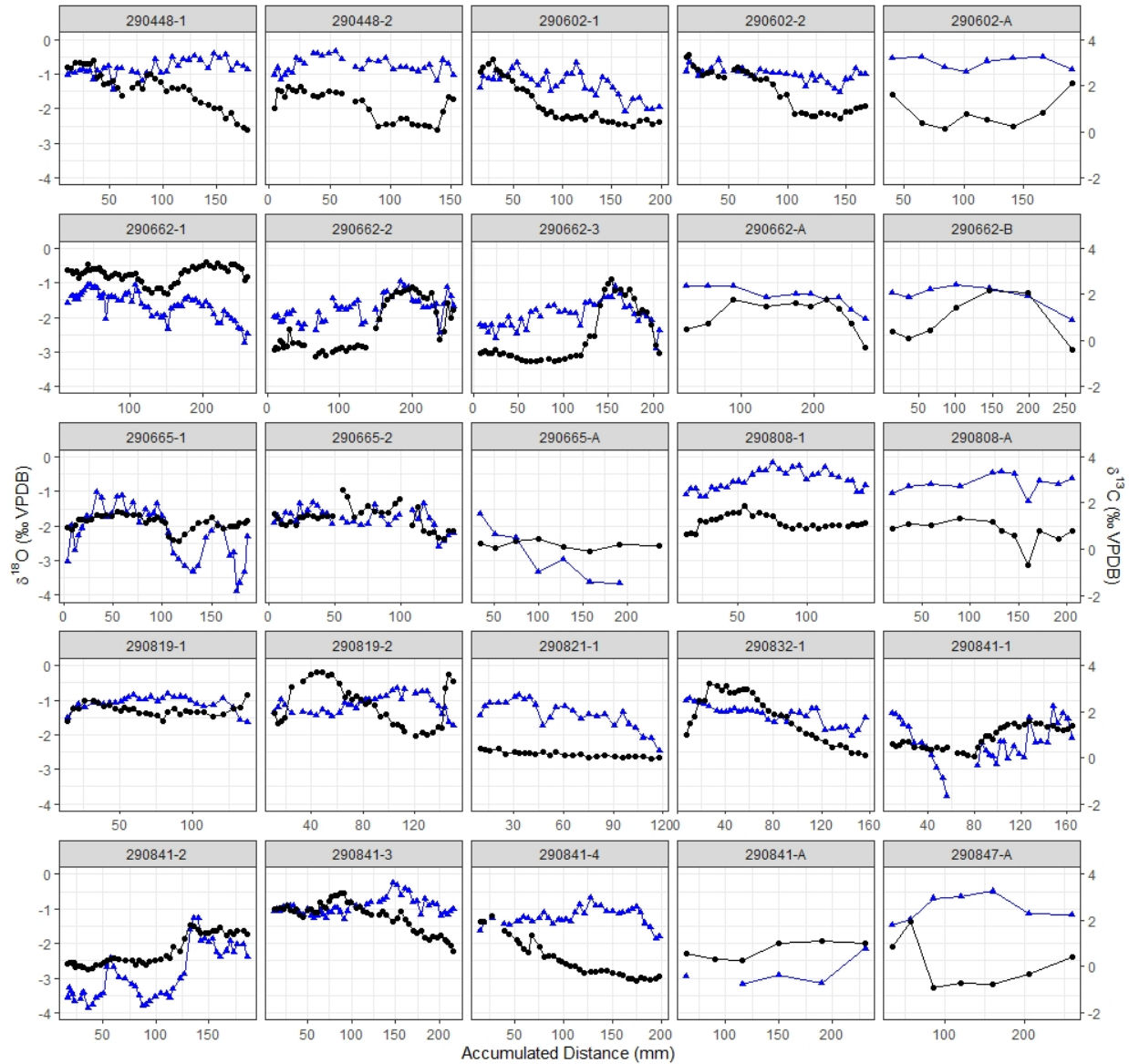
6B) Modern specimens
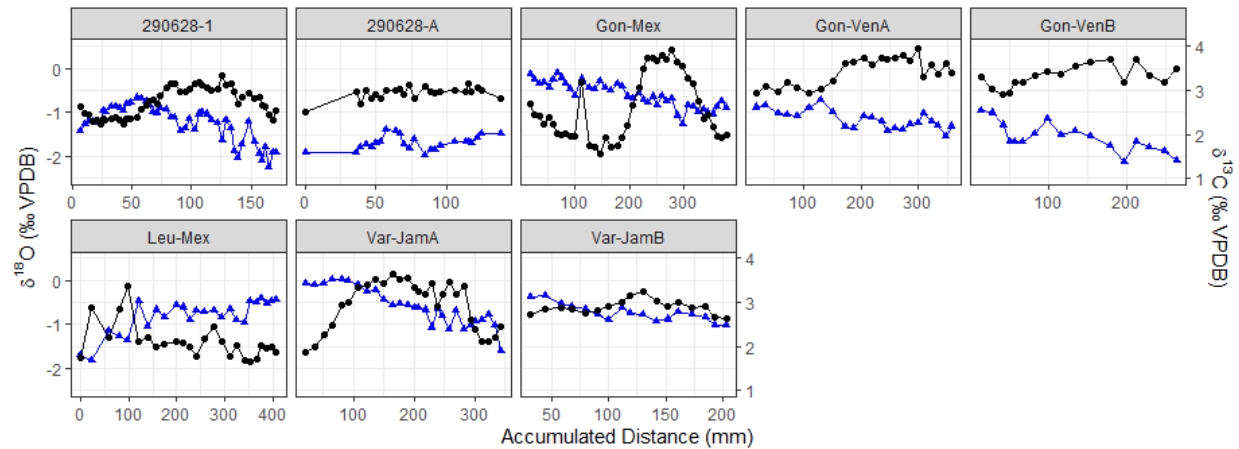
Supplemental Material Figure 7 (S7) – Comparison between δ^{18}O range and environmental parameters
Correlation between the range in δ^{18}O in each specimen and (A) the shell's stratigraphic height, (B) the interpreted paleosalinity, or (C) the inferred paleodepth. Paleosalinity and paleodepth taken from Hendy et al., 2015.
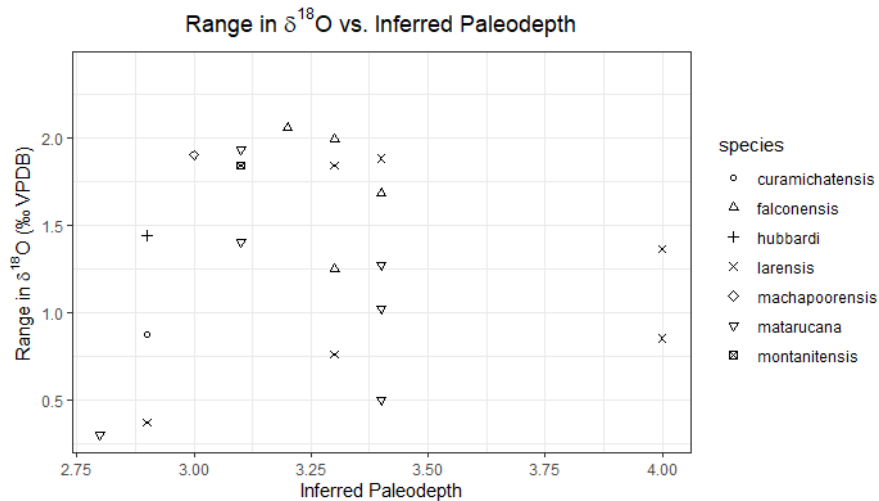
7A) Stratigraphic height vs. range in δ^{18}O in each shell, showing no correlation. Shells showing high (>1.5‰) ranges in δ^{18}O occur at all sampled horizons. Symbols represent the specific species of *Turritella*.

8
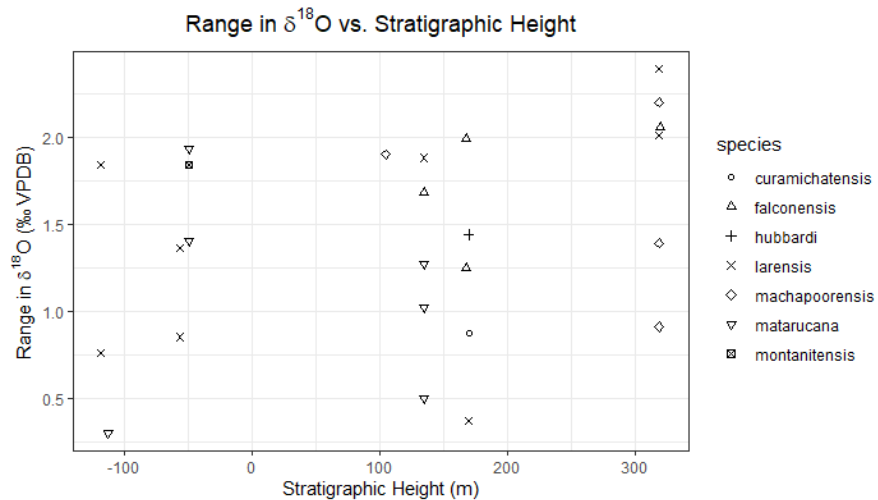
7B) Paleosalinity index vs. $\delta^{18}O$ range, showing no correlation. Salinity is in arbitrary units where 1=estuarine and 2=fully marine, numbers between 1 and 2 are the result of averaging all species in a given horizon for a determination of 'mostly marine' or 'mostly estuarine'. Paleosalinity values are taken from Hendy et al. 2015, and include more specimens than were analyzed here. Paleosalinity does not vary much below fully marine in the sampled horizons, and shells showing high (>1.5‰) ranges in $\delta^{18}O$ occur at 3 of 4 paleosalinity levels. Symbols represent the specific species of *Turritella*.
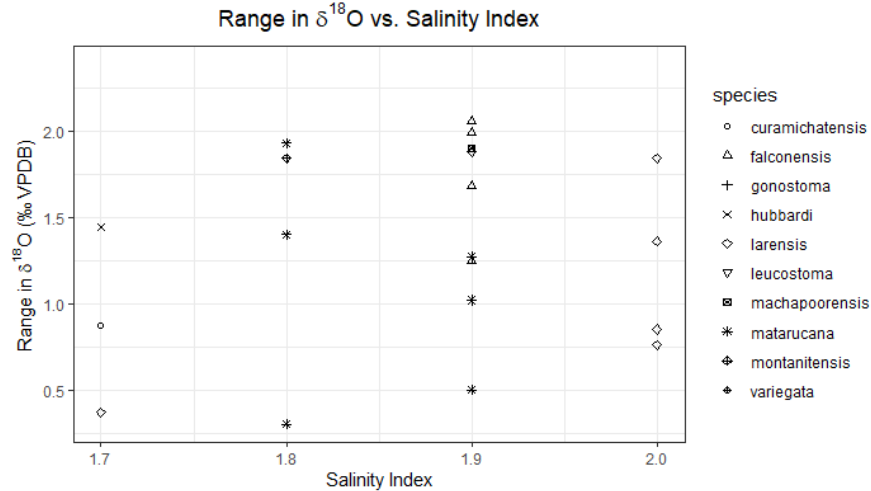

7C) Paleodeth index vs. $\delta^{18}O$ range, showing no correlation. Depth index is in arbitrary units where 1=intratidal, 2=shoreface (0-5m), 3=nearshore (5-15m), 4=inner shelf (15-50m), 5=mid shelf (5-100m), and 6=outer shelf (100-200m). Our samples range from (far) shoreface to the inner shelf, with most between 3-3.5 (nearshore). Shells showing high (>1.5‰) ranges in $\delta^{18}O$ occur at most paleodepth levels (3-3.5), with potentially reduced ranges at deeper depths (paleodepth = 4), however there are only a small number of samples at this depth. Symbols represent the specific species of *Turritella*.


9

Supplemental Material Figure 8 (S8) – Comparison between $\delta^{18}O$ range, shell size and lifespan

8A) Shell size. Range in $\delta^{18}O$ of each shell plotted against the total accumulated distance along the growth direction of each shell, a measurement of shell size, showing no correlation. Shells showing high (>1.5‰) ranges in $\delta^{18}O$ occur at all shell sizes between 150 and 375mm accumulated distance. Shells with accumulated distance less than 150mm show somewhat reduced range, although there are not many shells at this small size. Symbols represent the specific species of *Turritella*. There is not known to be any relationship between shell size and lifespan in turritellids (Allmon and Jones, 1992).
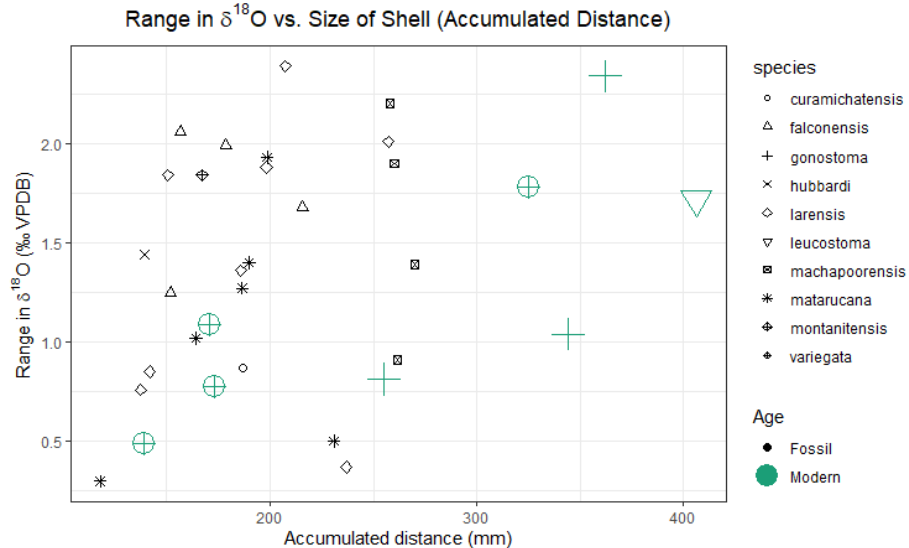

8B) Estimated lifespan. Range in $\delta^{18}O$ of each shell plotted against the estimated lifespan, showing no correlation. Shell lifespans were estimated based on $\delta^{18}O$ cyclicity, with the presence of a full sinusoid indicating a full year of life. Shell lifespans varied between <1 to 1.5 years as a minimum estimate (Table S2), in agreement with previous studies of Turritella (Allmon, 2011; Anderson et al., 2017). There is not known to be any relationship between shell size and lifespan in turritellids (Allmon and Jones, 1992). Symbols represent the specific species of *Turritella*.
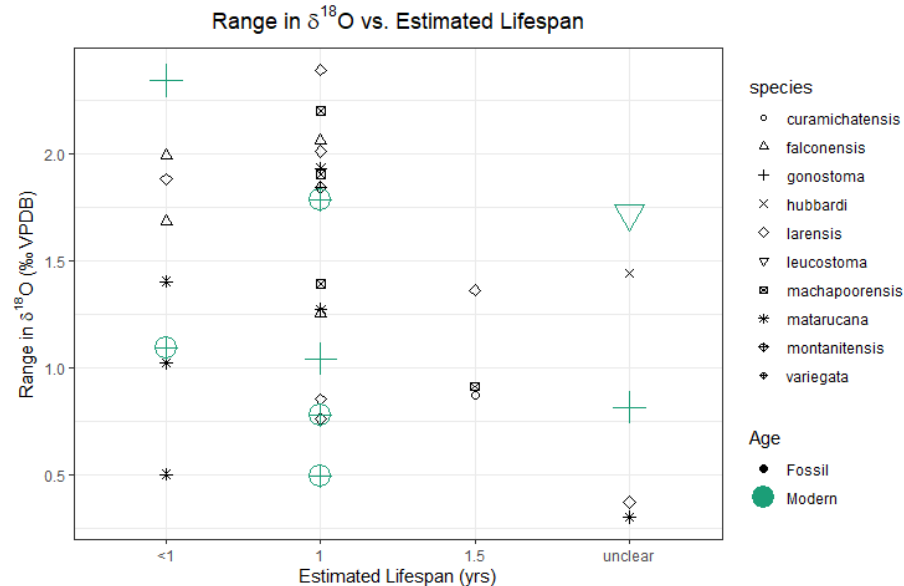
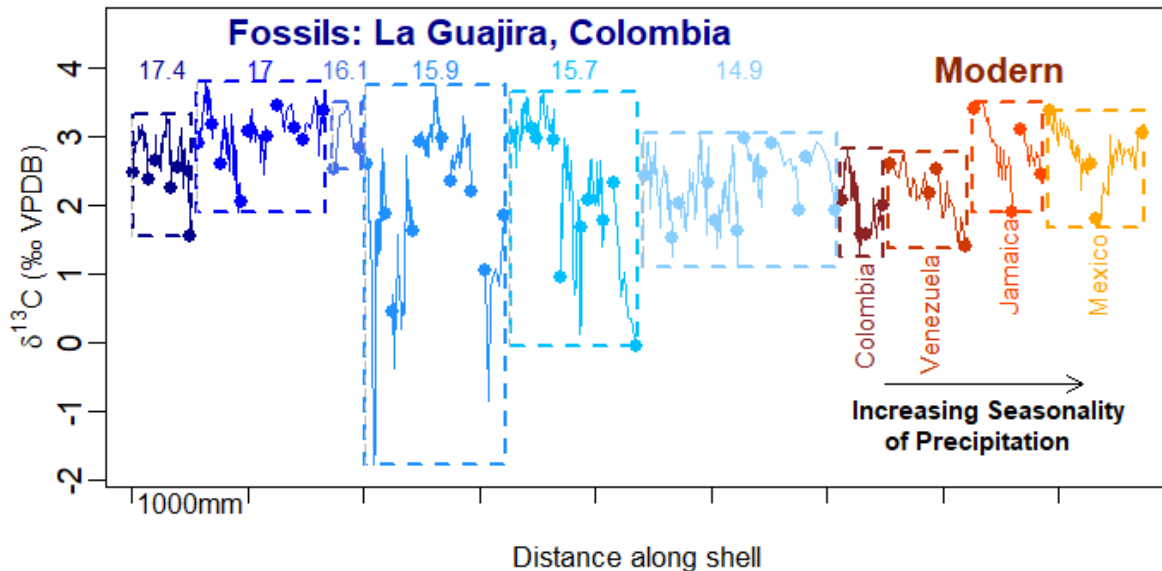**Supplemental Material Figure 9 (S9) – Seasonal variation in sea surface temperature at 4 modern sites**

Seasonal variation in sea surface temperature (SST, ºC) by month at each of the four modern sites. Data calculated from the NOAA ERSST v.5 gridded dataset. SST was averaged across the region (latitude-weighted), and then averaged in each month from 1930-2012.
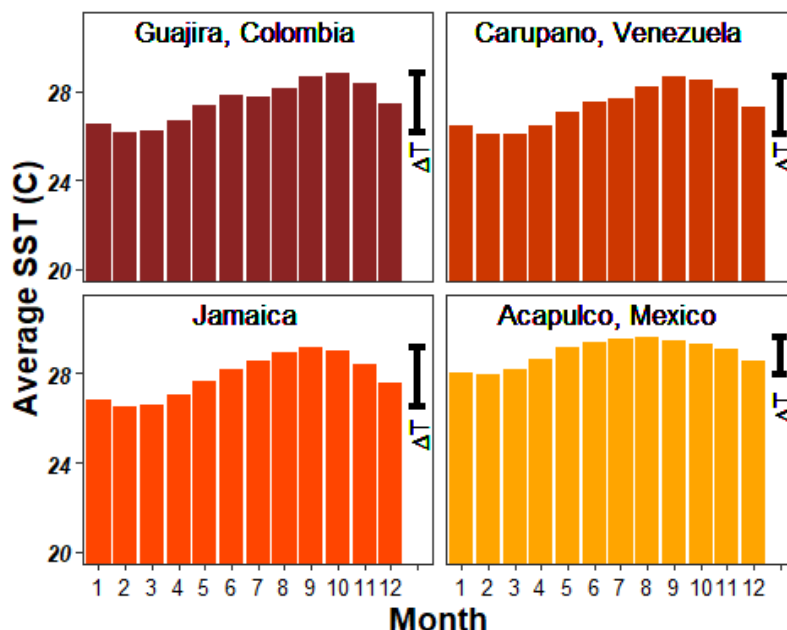
*NOAA_ERSST_V5 data provided by the NOAA/OAR/ESRL PSD, Boulder, Colorado, USA, at their website https://www.esrl.noaa.gov/psd*

Supplemental Material Figure 10 (S10) – δ^{13}C profiles of all shells

δ^{13}C sclerochronologies of all shells, plotted similar to Figure 2, which shows δ^{18}O. Fossil shells are arranged based on age of horizon. Modern shells are arranged by location, first showing Guajira Peninsula, and then in order of increasing precipitation seasonality. Boxes show range of maximum to minimum δ^{13}C for each modern location, or all fossil shells. X-axis represents the accumulated distance in the spiral direction around each shell: each shell's distance values were added to the previous to display them side by side. All values are in reference to VPDB.
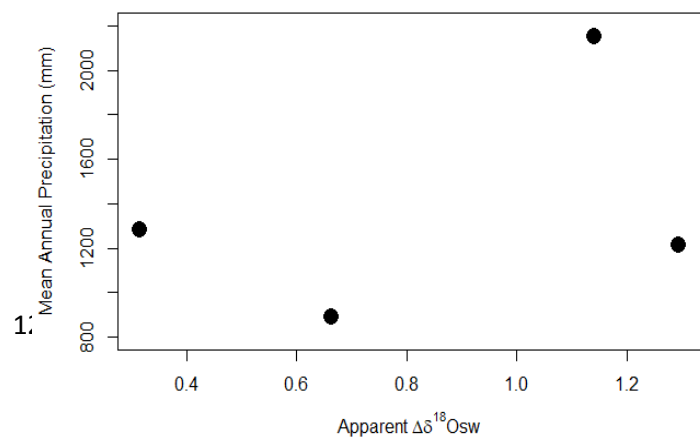
Supplemental Material Figure 11 (S11) – Correlation between range in δ^{13}C and range in δ^{18}O

Correlation is shown between range in δ^{13}C and range in δ^{18}O for all fossil and modern shells. No statistically significant correlation present (R^2 value of 0.01, p-value 0.24).
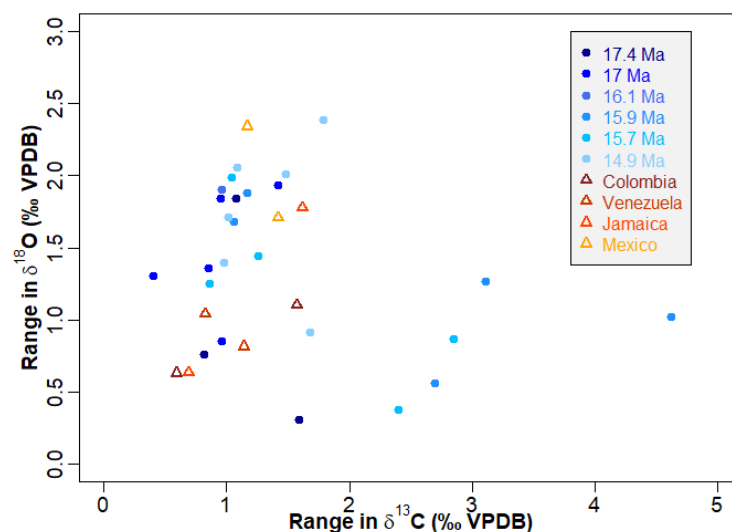
Supplemental Material Figure 12 (S12) – Correlation between apparent $\Delta\delta^{18}O_{sw}$ and Precipitation

Correlation is shown between apparent $\Delta\delta^{18}O_{sw}$ and seasonal precipitation variance (left), and mean annual precipitation (MAP, right), at each of the four modern sites. There is no correlation between apparent $\Delta\delta^{18}O_{sw}$ and MAP (right), but there is a strong correlation with seasonal precipitation variance (left). While four points is insufficient to be considered an empirically robust relationship, further research into this trend is warranted, as the strong correlation shows promise.


1

$$y = 138\,x + 99$$
$$R^2 = 0.98, \quad p = 0.011$$
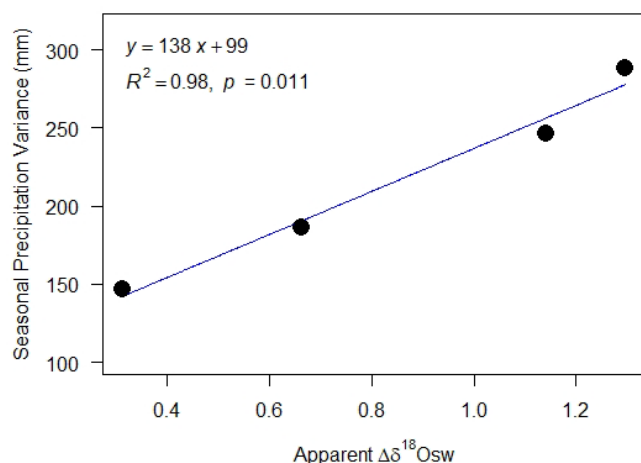
Supplemental Material Figure 13 (S13) – Raman spectroscopy of all samples

All fossil shells and 1 modern shell were scanned using Raman spectroscopy. We took point measurements using a Horiba XploRA PLUS Raman spectrometer paired with an Olympus BX41 microscope. The XploRA system is equipped with a 532 nm diode laser. We collected the spectra using a groove density of 1800 g/mm over a range of 100 to 1600 cm^{-1} at a laser power output of ~10 mW. We collected three scans per sample with a 3 second exposure time and 15 accumulations using a 50x long working distance objective. We used a polynomial baseline correction to remove background fluorescence in the LabSpec6 platform. The standards are sourced from the RRUFF database. Samples were mounted on microscope slides and stabilized in putty. Sample scans are included in the below figures as transparent gray lines. The RRuff standards for aragonite and calcite are plotted in pink and blue, respectively. All samples scanned had spectra clearly corresponding to aragonite, given the position and intensity of the peaks. The modern shell scans were not significantly different from fossil scans.
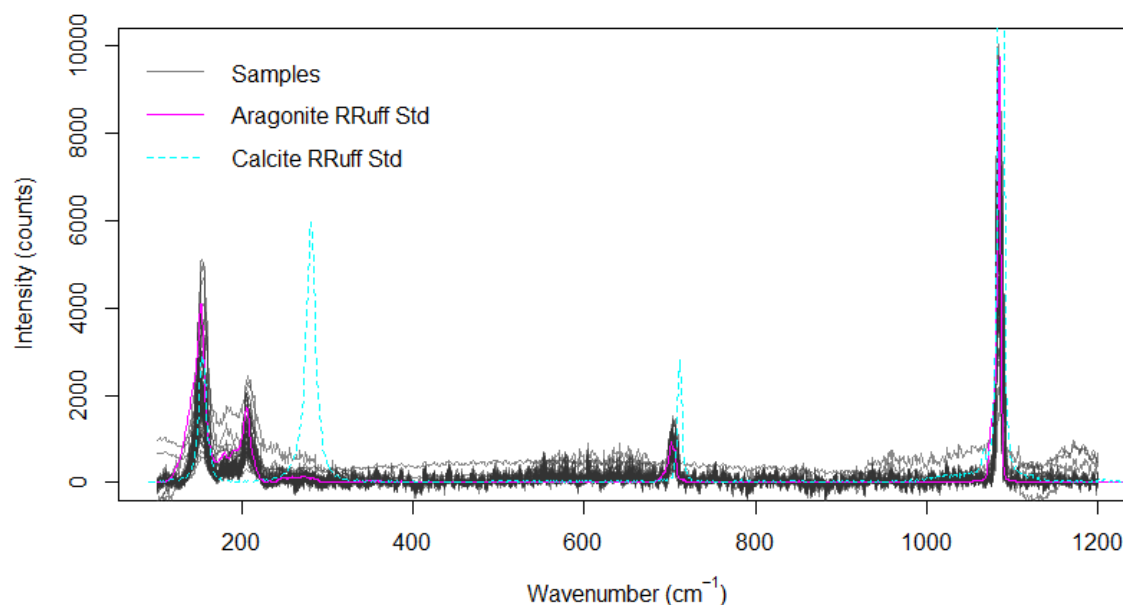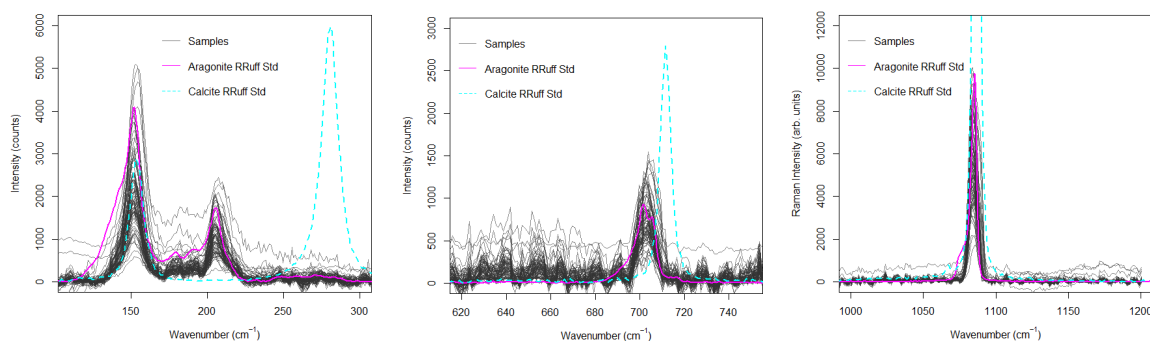
Supplemental Material Table S1 - Sample IDs, STRI locality numbers, stratigraphic heights and calibrated ages for all measured specimens.

For samples collected on the Guajira peninsula (all fossil specimens and two modern), the sample name is structured as the STRI locality ID, followed by the specimen identifier, which is either a number if named by Universidad del Norte (UdN), or a letter if named by University of Michigan (UofM). Modern samples are in shaded gray cells. Sample not analyzed for stable isotopes and only used for XRD have a locality number followed by an X, and XRD is specified in the Resolution column. For modern Turritella specimen not collected on the Guajira peninsula, the sample name is a shorted form of the species and location (country) collected from.

Sample Name	Reso-lution	Locality STRI ID	Age	Calibrated Age	Unit	Strat. Height	Species	Location
290819-1	High	290819	Burdigalian	17.4	Jimol	-118	*T. larensis*	Guajira
290819-2	High	290819	Burdigalian	17.4	Jimol	-118	*T. larensis*	Guajira
290821-1	High	290821	Burdigalian	17.4	Jimol	-112	*T. matarucana*	Guajira
290808-1	High	290808	Burdigalian	17.0	Jimol	-56	*T. larensis*	Guajira
290602-1	High	290602	Burdigalian	17.0	Jimol	-49	*T. matarucana*	Guajira
290602-2	High	290602	Burdigalian	17.0	Jimol	-49	*T. montanitensis*	Guajira
290841-1	High	290841	Langhian	15.9	Castilletes	135	*T. matarucana*	Guajira
290841-2	High	290841	Langhian	15.9	Castilletes	135	*T. matarucana*	Guajira
290841-3	High	290841	Langhian	15.9	Castilletes	135	*T. falconensis*	Guajira
290841-4	High	290841	Langhian	15.9	Castilletes	135	*T. larensis*	Guajira
290448-1	High	290448	Langhian	15.7	Castilletes	168	*T. falconensis*	Guajira
290448-2	High	290448	Langhian	15.7	Castilletes	168	*T. falconensis*	Guajira
290665-1	High	290665	Langhian	15.7	Castilletes	170	*T. curamichatensis*	Guajira
290665-2	High	290665	Langhian	15.7	Castilletes	170	*T. hubbardi*	Guajira
290662-1	High	290662	Langhian	14.9	Castilletes	319	*T. machapoorensis*	Guajira
290662-2	High	290662	Langhian	14.9	Castilletes	319	*T. larensis*	Guajira
290662-3	High	290662	Langhian	14.9	Castilletes	319	*T. larensis*	Guajira
290832-1	High	290832	Langhian	14.9	Castilletes	320	*T. falconensis*	Guajira
290602-A	Coarse	290602	Burdigalian	17.0	Jimol	-49	*T. matarucana*	Guajira
290662-A	Coarse	290662	Langhian	14.9	Castilletes	319	*T. machapoorensis*	Guajira
290662-B	Coarse	290662	Langhian	14.9	Castilletes	319	*T. machapoorensis*	Guajira
290665-A	Coarse	290665	Langhian	15.7	Castilletes	170	*T. larensis*	Guajira
290808-A	Coarse	290808	Burdigalian	17.0	Jimol	-56	*T. larensis*	Guajira

290841-A	Coarse	290841	Langhian	15.9	Castilletes	135	*T. matarucana*	Guajira
290847-A	Coarse	290847	Burdigalian	16.1	Castilletes	105	*T. machapoorensis*	Guajira
290628-1	High	290628	Modern	Modern	Modern	Modern	*T. variegata*	Guajira
290628-A	High	290628	Modern	Modern	Modern	Modern	*T. variegata*	Guajira
Gon-Mex	High	N/A	Modern	Modern	Modern	Modern	*T. gonostoma*	Mexico
Leu-Mex	High	N/A	Modern	Modern	Modern	Modern	*T. leucostoma*	Mexico
Gon-VenA	High	N/A	Modern	Modern	Modern	Modern	*T. gonostoma*	Venezuela
Gon-VenB	High	N/A	Modern	Modern	Modern	Modern	*T. gonostoma*	Venezuela
Var-JamA	High	N/A	Modern	Modern	Modern	Modern	*T. variegata*	Jamaica
Var-JamB	High	N/A	Modern	Modern	Modern	Modern	*T. variegata*	Jamaica
290602-X	XRD	290602	Burdigalian	17.0	Jimol	-49	*T. matarucana*	Guajira
290841-X	XRD	290841	Langhian	15.9	Castilletes	135	*T. matarucana*	Guajira
290665-X	XRD	290665	Langhian	15.7	Castilletes	170	*T. curamichatensis*	Guajira
290832-X	XRD	290832	Langhian	14.9	Castilletes	320	*T. machapoorensis*	Guajira

Supplemental Material Table S2 – Raw $\delta^{18}O$ and $\delta^{13}C$ data for all shells
All individual $\delta^{18}O$ and $\delta^{13}C$ values are included in a supplementary Excel table.

Supplemental Material Table S3 – Shell lifespan, size, and $\delta^{18}O$ and $\delta^{13}C$ range for all shells
This table contains columns for sample number, *Turritella* species, estimated lifespan, size (represented by total spiral distance around the shell), and max-to-min range in $\delta^{18}O$ and $\delta^{13}C$. Cells shaded gray are modern samples.

Sample Name	Species	Lifespan (yrs)	Total acc. distance (mm)	$\delta^{13}C$ range (‰ VPDB)	$\delta^{18}O$ range (‰ VPDB)
290819-1	*T. larensis*	1	137.4	0.80	0.76
290819-2	*T. larensis*	1	150.6	1.08	1.84
290821-1	*T. matarucana*	unclear	118.0	1.59	0.30
290808-1	*T. larensis*	1	141.9	0.96	0.85
290602-1	*T. matarucana*	1	198.6	1.42	1.93
290602-2	*T. montanitensis*	1	167.1	0.95	1.84
290841-1	*T. matarucana*	<1	164.1	4.62	1.02
290841-2	*T. matarucana*	1	186.5	3.11	1.27
290841-3	*T. falconensis*	<1	215.8	1.06	1.68
290841-4	*T. larensis*	<1	198.3	1.17	1.88
290448-1	*T. falconensis*	<1	178.7	1.04	1.99
290448-2	*T. falconensis*	1	152.0	0.86	1.25
290665-1	*T. curamichatensis*	1.5	186.7	2.85	0.87
290665-2	*T. hubbardi*	unclear	139.6	1.26	1.44
290662-1	*T. machapoorensis*	1.5	261.6	1.68	0.91
290662-2	*T. larensis*	1	257.2	1.50	2.01
290662-3	*T. larensis*	1	207.4	1.79	2.39
290832-1	*T. falconensis*	1	156.9	1.09	2.06
290602-A	*T. matarucana*	<1	190.0	0.60	1.40
290662-A	*T. machapoorensis*	<1	270.0	0.98	1.39
290662-B	*T. machapoorensis*	1	258.0	1.01	2.20
290665-A	*T. larensis*	unclear	237.0	2.35	0.37

290808-A	*T. larensis*	1.5	186.0	0.8	1.36
290841-A	*T. matarucana*	<1	231.0	2.70	0.50
290847-A	*T. machapoorensis*	1	260.0	0.96	1.90
290628-1	*T. variegata*	1	171.0	1.58	1.09
290628-A	*T. variegata*	<1	139.0	0.25	0.49
Gon-Mex	*T. gonostoma*	1	362.0	1.18	2.34
Leu-Mex	*T. leucostoma*	unclear	406.0	1.42	1.72
Gon-VenA	*T. gonostoma*	1	344.0	0.83	1.04
Gon-VenB	*T. gonostoma*	unclear	255.0	1.14	0.81
Var-JamA	*T. variegata*	1	325.0	1.66	1.78
Var-JamB	*T. variegata*	<1	173.0	0.76	0.78

Supplemental Material Table S4 – Modern climate data for all sites

Air temperature data was obtained for several nearby stations to the sampling site, and is based on NOAA Daily Summaries (Venezuela, Jamaica and Mexico) and IDEAM historical data (Colombia). Sea surface temperature data was obtained from instrumental records (see sources below table), was also calculated using the ERSST v. 5 global gridded model for comparison (Huang et al., 2017). Calculations were made by averaging by month over the period 1930-2012, and the resulting range is the average seasonal temperature range. The same time period was used to determine precipitation from the CRU 3.25 Global Precipitation dataset (Harris et al., 2014). Seasonal variance in air temperature (ΔT), SSTs (ΔSST) and precipitation (seasonal variance) was calculated by taking the difference of the highest and lowest average monthly values.

	Air Temperature Data: NOAA Daily Summaries, IDEAM Historical Data			SSTs: Local, Instrumental Data		SSTs: ERSST v.5 Gridded Dataset		Precipitation: CRU 3.25 Gridded Dataset	
Location	MAT (°C)	Seasonal T Range	ΔT Annual	Seasonal T Range	ΔSST Annual	Mean annual SST	ΔSST Annual	MAP (mm)	seasonal variance (mm)
Castilletes, La Guajira, CO	**28.2**	**26.8-29.1**	**2.3**	**24.9-27.9** *(a)*	**3.0**	**27.5**	**2.65**	**892**	**186**
Nazareth, CO	27.1	25.7-27.8	2.1						
Pto Bolivar, CO	28.4	27.0-29.3	2.3						
Rancho Grande, CO	29	27.8-29.9	2.1						
Carupano, VE	**27.5**	**26.3-28.3**	**2**	**23.4-26.8** *(b)*	**3.4**	**27.3**	**2.58**	**1282**	**147**
Antonio Jose de Sucre, VE	27.6	26.6-28.4	1.8						
Guiria, VE	27.7	26.6-28.5	1.9						
Piarco Intl Airport, TD	27.1	26.0-27.8	1.8						
Porlamar Intl Airport, VE	27.7	26.0-28.4	2.4						
Jamaica	**27.4**	**25.9-28.8**	**2.9**	**26.5-29.5** *(c)*	**3.0**	**27.9**	**2.65**	**2153**	**246**
Montego Bay,	27	25.4-	2.9						

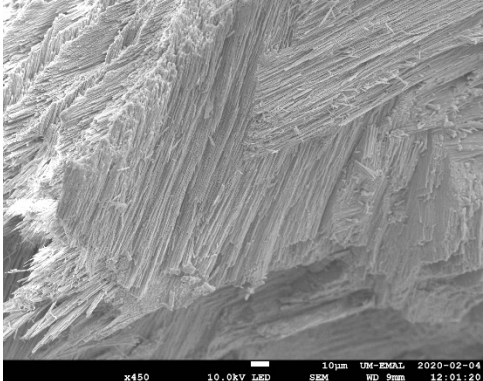|									
JM		28.3							
Norman Manley Intl, JM	27.8	26.3-29.3	2.9						
Acapulco, MX	**27.7**	**26.5-28.9**	**2.4**	**25.6-30.5** *(d)*	**4.9**	**28.9**	**2.1**	**1215**	**288**

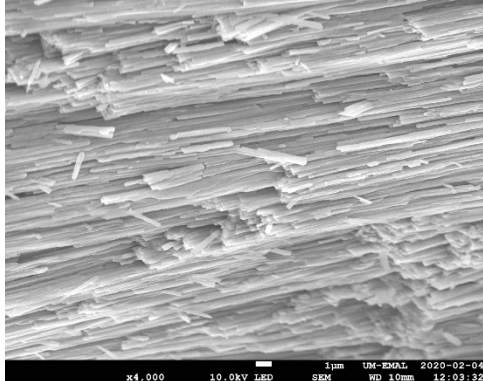(a) Montoya-Sánchez et al., 2018
(b) Jury, 2018
(c) Gates, 1990
(d) Rojas-Herrera et al., 2016; Moreno-Díaz et al., 2015
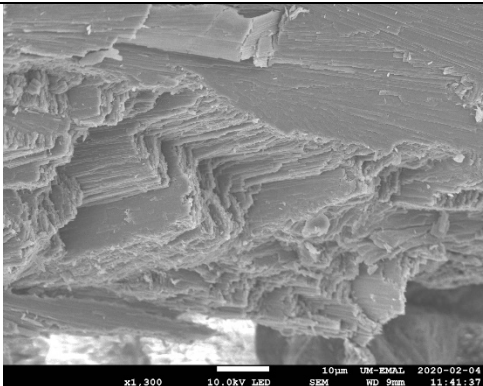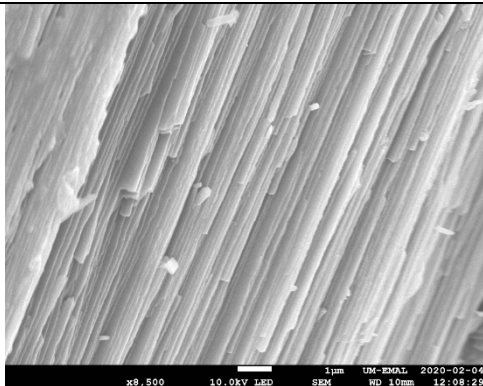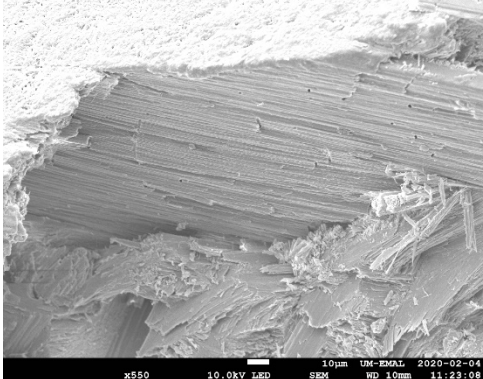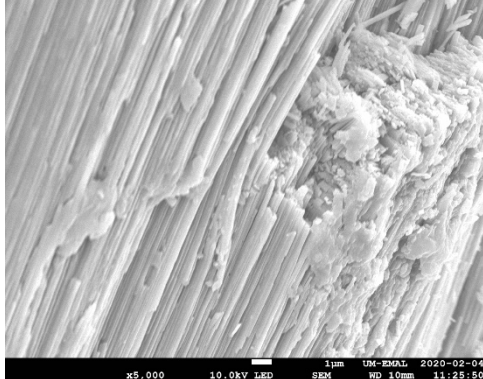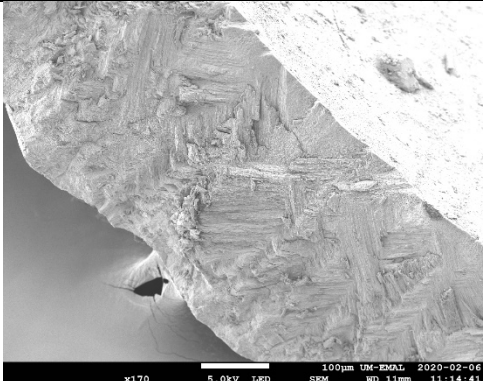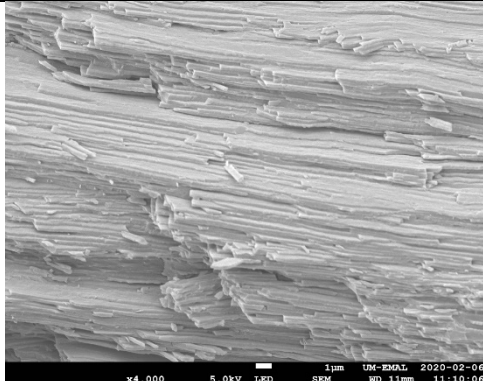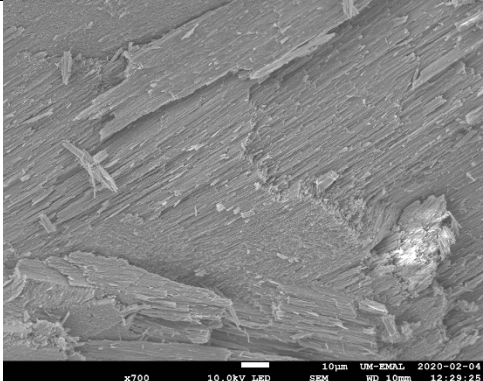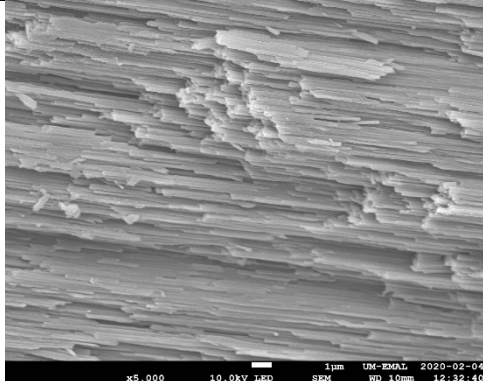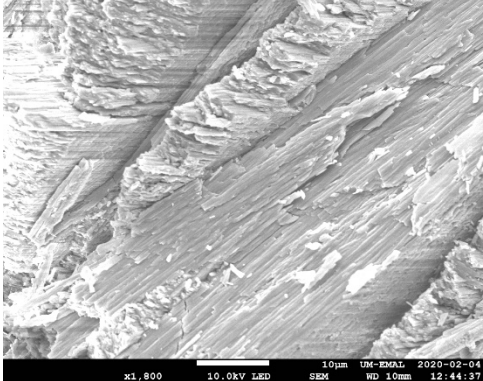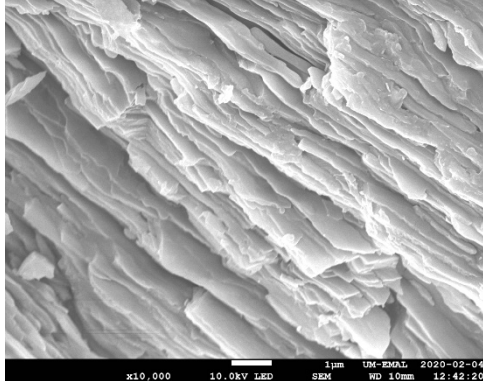
NOAA_ERSST_V5 data provided by the NOAA/OAR/ESRL PSD, Boulder, Colorado, USA, at their website https://www.esrl.noaa.gov/psd/
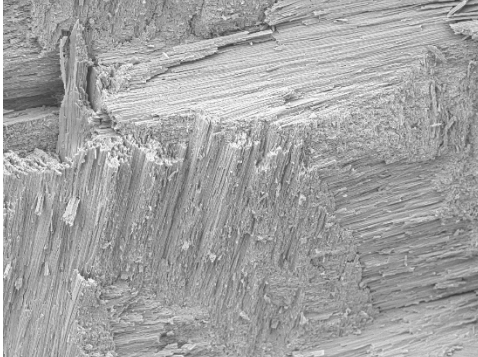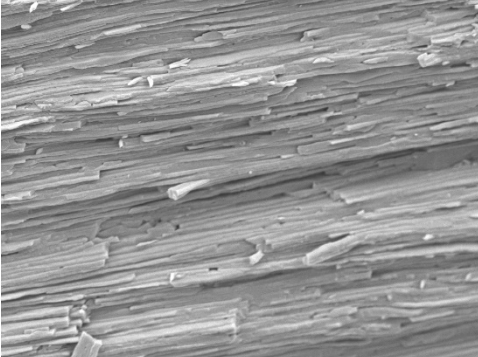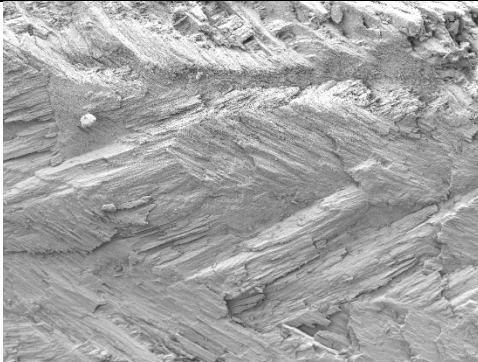
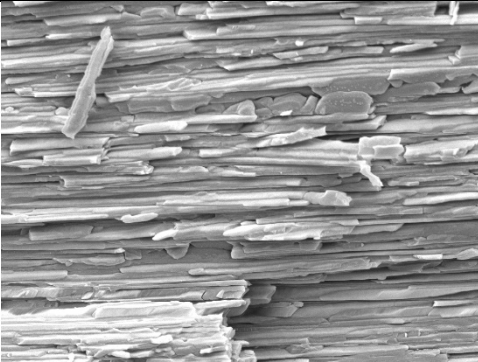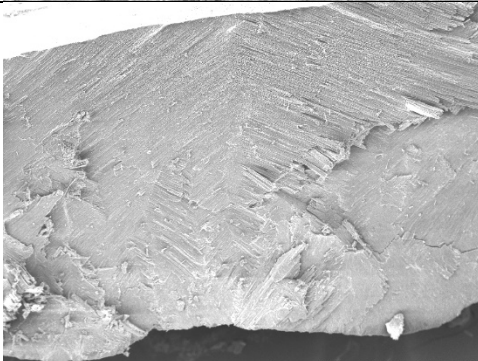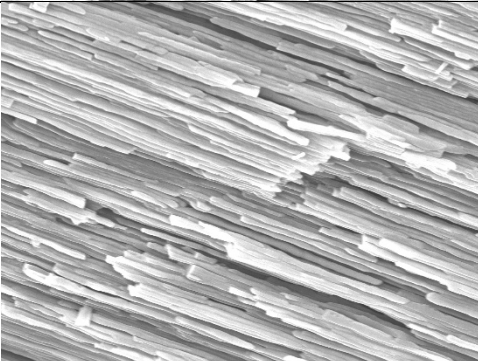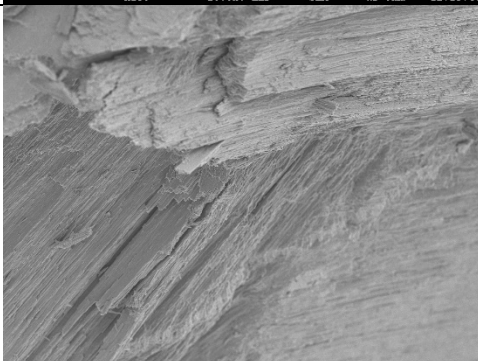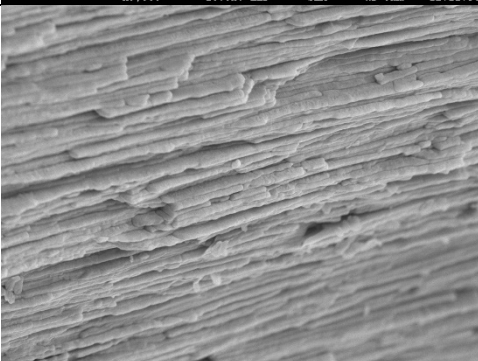## Supplemental Material Table S5 – SEM imagery

SEM imagery of fossil samples showed preservation of the original aragonitic shell fabric, which is visually very similar to the fabric observed in modern samples (top 3 rows). Fossil samples also preserve larger-scale cross-lamellar growth patterns, common in gastropods, and documented in the left column of images. Both of these structures are indicative of original, biogenic aragonite. Images were taken on a freshly broken face, broken off from near the shell aperture.

Sample name	Image 1 (cross-lamellar growth pattern)	Image 2 (detail of shell fabric)
290628-1 (modern)		
290628-A (modern)		

Var-JamB (modern)		
290448-1		
290602-1		
290662-3		

290662-A			
290665-A			
290808-1			
290819-1			

290821-1			
290832-1			
290841-1			
290841-3			

Additional References not cited in the Main Text

Andrade, C.A., and Barton, E.D., 2005, The Guajira upwelling system: Continental Shelf Research, v. 25, p. 1003–1022, doi:10.1016/j.csr.2004.12.012.

Gates, R.D., 1990, Seawater temperature and sublethal coral bleaching in Jamaica: Coral Reefs, v. 8, p. 193–197, doi:10.1007/BF00265010.

Harris, I., Jones, P.D., Osborn, T.J., and Lister, D.H., 2014, Updated high-resolution grids of monthly climatic observations - the CRU TS3.10 Dataset: Journal of Climatology, v. 34, p. 623–642, doi:10.1002/joc.3711.

Huang, B., Thorne, P.W., Banzon, V.F., Boyer, T., Chepurin, G., Lawrimore, J.H., Menne, M.J., Smith, T.M., Vose, R.S. and Zhang, H., 2017, NOAA Extended Reconstructed Sea Surface Temperature (ERSST), Version 5. 1930-2016. NOAA National Centers for Environmental Information. doi:10.7289/V5T72FNM.

IAEA/WMO, 2018, Global Network of Isotopes in Precipitation: The GNIP Database, Accessible at: https://nucleus.iaea.org/wiser

Johnson E.H., Anderson, B.M., and Allmon, W.D., 2017, What can we learn from all those pieces? Obtaining data on drilling predation from fragmented high-spired gastropod shells, *Palaios* v. 32, p. 271-277. doi: 10.2110/palo.2016.088

Jury, M.R., 2018, Eastern Venezuela coastal upwelling in context of regional weather and climate variability: Regional Studies in Marine Science, v. 18, p. 219–228, doi:10.1016/j.rsma.2017.10.010.

Montoya-Sánchez, R.A., Devis-Morales, A., Bernal, G., and Poveda, G., 2018, Seasonal and intraseasonal variability of active and quiescent upwelling events in the Guajira system, southern Caribbean Sea: Continental Shelf Research, v. 171, p. 97–112, doi:10.1016/j.csr.2018.10.006.

Moreno-Díaz, G., Rojas-Herrera, A.A., Violante-González, J., González-González, J., Acevedo, J.L.R., and Ibáñez, S.G., 2015, Temporal Variation in Composition and Abundance of Phytoplankton Species during 2011 and 2012 in Acapulco Bay, Mexico: Open Journal of Marine Science, v. 05, p. 358–367, doi:10.4236/ojms.2015.53029.

Rojas-Herrera, A.A., Violante-González, J., García-Ibáñez, S., Villerías-Salinas, S., and Moreno-Díaz, G., 2016, Temporal Variation of the Pelagic Copepod Community in Acapulco Bay, Mexico: Open Journal of Marine Science, v. 06, p. 40–48, doi:10.4236/ojms.2016.61005.